JOURNAL OF PROPULSION AND POWER
Vol. 27, No. 2, March–April 2011

Effect of Fluid/Structure Coupling on Unstable Mechanisms in a Solid Rocket Motor

Renato Nunes*
Instituto Tecnológico de Aeronáutica , 12228-901 São José dos Campos, Brazil
and
Frédéric Plourde†
Ecole Nationale Supérieure de Mécanique et d'Aérotechnique, 86960 Chasseneuil, France

DOI: 10.2514/1.48639

The influence of fluid/structure coupling in a subscale model has been investigated in the framework of solid rocket motor instability. The first self-sustained oscillations of the flexible membrane were identified, and it was found that the flapping motion strengthens the laminarization process in the obstacle's wake vortex shedding. In addition, the equilibrium between vortices in the shear layer and wall vortex shedding is modified and instability is favored by introducing a flexible membrane. Introduction of the forced oscillating motion of the inhibitor gives rise to similar conclusions. However, a significant lessening of the unstable process was noted when the flexible membrane exhibited specific characteristics.

Nomenclature

a = sound velocity, m/s
E_p = thickness of the rigid inhibitor, m
f_n = $na/2L$, nth longitudinal acoustic mode, Hz
H = nozzle height, m
H_c = channel height, m
I_T = turbulence intensity, $\sqrt{\bar{u}'^2 + \bar{v}'^2}/aM$
L = channel length, m
M = characteristic Mach number based on the mass flow rate, $q_m/a\rho w H_c$
P = static pressure, Pa
q_m = total mass flow rate, kg/s
$R_{x'y'}$ = correlation coefficient of arbitrary functions of time x' and y', $\overline{x'(t)y'(t+\tau)}/\sqrt{\overline{x'^2(t)}}\sqrt{\overline{y'^2(t)}}$
$S_{x'}$ = $s_{x'}/\bar{x}'_2$, normalized power spectral density, Hz^{-1}
$s_{x'}$ = power spectral density
T = period, s
$\bar{U}$ = normalized mean velocity in each section, $\bar{u}/U_0$
U_o = characteristic velocity, m/s
u, v = velocity component in X and Y directions, m/s
$\bar{u}$ = mean velocity in each section, m/s
w = channel width, m
X, Y = nondimensional axes normalized by H_c
ε = membrane thickness normalized by E_p
ρ = density, kg/m^3
τ = time delay, s
Ω_z = vorticity normalized by U_o/H_c
$\bar{\ }$ = time-averaged
$\langle\,\rangle$ = phase-averaged

Superscript

$'$ = fluctuating component

I. Introduction

THE unstable mechanisms arising in solid rocket motors (SRMs) have been widely studied in both numerical and experimental investigations, and it is now a commonly established fact that segmented motor instability is mainly driven by two vortex-shedding phenomena. Because of the presence of an inhibitor between propellant blocks, surface restriction favors shear-layer development in the inhibitor's wake, where vortex shedding arises. Vortices travel up to the motor's rear end and impinge upon the submerged nozzle. Impingement induces pressure waves convected toward the SRM head end; during such convection, it may directly interfere with shear-layer development by modulating its own shedding frequency. As soon as aeroacoustic coupling is locked, a resonant state is established and unstable levels attain their highest rates.

Dotson et al. [1] analyzed pressure oscillation measurements during static firing tests of the TITAN IV SRMU and convincingly suggested the existence of aeroacoustical coupling between the motor's fundamental acoustic nodes and vortices arising from the cavity between the center and aft segments. Similar conclusions were deduced from static firing tests of the Ariane 5 SRM [2]. Flatau and Van Moorhem [3] fully detailed the vortex shedding as a source of sound within segmented chambers and such an interaction was examined for several experimental conditions; the authors explicitly demonstrated that the baffle-to-nozzle acoustic modes are the dominant mechanism responsible for the lock-in of the velocity-pressure couplings. In addition, we wish to underline that not only the vortex-shedding mechanisms due to SRM segmentation function on their own as an unstable source and that gaseous production along the propellant blocks directly interacts in the unstable process. From a theoretical point of view, temporal vortex concentration along injecting walls was taken into close account by both Griffond and Casalis [4] and Zhao and Kassoy [5]. Zhao and Kassoy [5] proposed a mathematical formulation to describe the evolution of vorticity at a low Mach number with weakly viscous internal flow sustained by mass addition along the cylindrical porous wall; the formulation allowed them to depict vorticity development and to shed light on the significant vorticity distribution magnitude present in the transient process. Griffond and Casalis [4] developed a nonparallel Taylor flow stability analysis enabling them to depict the unstable mechanisms exhibited in subscale cold-gas setup. As far as we know, the wall vortex-shedding phenomenon in SRM was first put forward by Brown et al. [6] as a factor in a cold-gas setup, and numerical simulations [7] have confirmed the contribution of wall vortex shedding to unstable activity. In addition, interaction between the two vortex-shedding mechanisms is driven by both internal dynamic

---

Received 4 January 2010; revision received 30 August 2010; accepted for publication 29 August 2010.

*Space Propulsion Division.

†Institut P Prime, UPR CNRS No. 3346.

conditions and the tilted angle of the propellant block; this conclusion was recently drawn by Nguyen et al. [8].

As was clearly put forward by Najjar et al. [9], the mechanisms that interact with SRM instability are numerous and complex, and the pronounced interaction of basic physical features renders its description even more difficult. Propellant combustion and erosive combustion, turbulence, and two-phase flow contribution due to alumina particles are just some examples of basic physics that come to play in SRMs. Taking into account not only the significant flowfield load on inhibitors, but also the fluctuating activity in the whole flowfield, fluid/structure coupling in SRM is not an easy task to tackle. And yet, estimation of its potential contribution to whole flowfield instability is one of the next major identified steps in ongoing research. In regard to this objective, several questions need to be addressed: Does inhibitor flexibility interact directly on unstable levels? Or else, on the contrary, does flexible inhibitor act as a means of controlling and reducing unstable modes in SRM? The identification of potential fluid/structure contribution in SRM is by no means easy, but one possible approach consists of conducting dedicated numerical simulations so as to study such coupling. That is how effects on the flowfield near a joint slot in a typical large SRM were analyzed by Fiedler et al. [10] In their paper, the researchers successfully computed the motion of a flexible inhibitor located in the core flow region aft of a joint slot in a fully coupled 3-D simulation. They convincingly demonstrated that an inhibitor flaps periodically with an angle of deflection ranging from 30 to 40 deg. Unfortunately, no information regarding such a flapping effect on the unstable mechanisms is available as of yet and according to the authors, simulations shall have to be improved in order to better depict fluid/structure interaction. It should be added that though numerical capability has significantly grown over recent decades and become an essential tool of development, experimental data remain necessary not only for validation purposes, but also in analysis of potential interaction in the unstable process of SRMs. With that in mind, Fouilhac et al. [11] focused on an experimental airflow setup designed to study interaction between a jet and a flexible membrane. To simulate aeroacoustic coupling, a loudspeaker produced acoustic waves and several membranes were tested. The results clearly demonstrate that resonance may be explained as the natural response of the membrane and that aeroacoustical resonance likewise induces vibrations on the latter. This key finding must be analyzed in an SRM framework so as to determine the way in which fluid/structure coupling either directly or indirectly impinges upon the unstable mechanisms identified in a typical internal flowfield.

In this paper, we wish to emphasize the impact of fluid/structure coupling on the whole solid rocket motor characteristic flow and, more specifically, on the unstable mechanisms that literally drive large SRM chamber unsteadiness. Although an analysis is being conducted, the MICAT (Montage Investigation Couplage Acoustique Tourbillons) cold-gas setup [12–14] guarantees many essential features of SRM flowfield characteristics (wall-injection flow, segmented and confined areas, potentially strong aeroacoustic coupling, etc.) and the rigid inhibitors used up until now were replaced in our experiment by flexible membranes. Several membranes were studied; they had been chosen so as to submit several natural frequencies of the membrane in the range of acoustic longitudinal modes. In the framework of this key analysis, one drawback may nonetheless be identified: the use of a flexible membrane does not provide a given excitation process for the flowfield (i.e., the induced oscillation undergoes no control). And so, in order to monitor oscillation input, a mechanical vibration system was developed and adapted to the experimental setup; it had been designed to endow the rigid inhibitor with an oscillation motion at a given frequency and amplitude. Once the inhibitor is forced, it is possible to estimate the effects of inhibitor vibration on the unstable mechanisms before proceeding to analysis of natural and flexible membrane effects.

II. Experimental Setup and Measurement Systems

All the results presented hereinafter were obtained experimentally with the aim of depicting possible fluid/structure coupling influence on SRM instability. The experiments were carried out with the MICAT cold-gas setup [11–13] dedicated to large segmented SRM instability analysis. The model ($L = 0.623$ m) was designed to reproduce the main geometric and dynamic characteristics of Ariane 5 segmented motors: i.e., segmented blocks and submerged nozzle. The model was bidimensional and lent itself to experimental

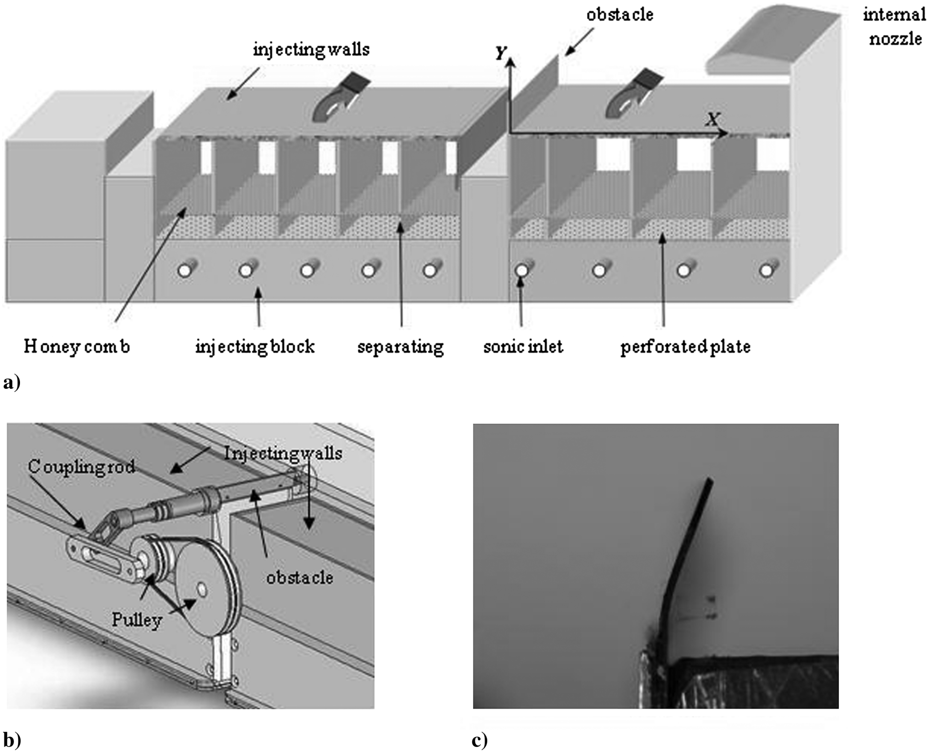

Fig. 1 MICAT experimental setup: a) schematic view, b) presentation of the mechanical system forcing oscillating motion of a straight and rigid inhibitor, and c) view of the $e = 0.5$ flexible obstacle for $M = 0.095$ flow conditions.

investigations; as shown in Fig. 1, two injecting blocks were located in the chamber separated by an embedded obstacle. Propellant block combustion was simulated by injecting air at ambient temperature through a 2-μm-diam sintered-bronze sphere; mass flow rate uniformity was controlled by a feeding system consisting of several sonic inlet injectors, a honeycomb, and isolated cells feeding a specific porous wall surface. The porosity and thickness of the porous plate allowed for isolation of injecting noise from pressure signals generated by the flow to be studied. A submerged nozzle was located at the rear part of the chamber to ensure the acoustic isolation of the chamber from the outer environment; the height of the nozzle throat could be varied, thereby controlling the characteristic Mach number M.

Fluid/structure effect of the inhibitor was studied from two different angles. The first was generated by replacing the rigid inhibitor with a flexible one. Up until now, all experimental studies on the MICAT setup have been carried out without any inhibitor vibration; the inhibitor was made of steel whose mechanical characteristics prevented the latter. In our experiment, however, a flexible inhibitor [i.e., a nitrilic elastomer (33% acrylonitrile)] was introduced in the MICAT setup, instead of the rigid one. Several membranes were tested and only their thickness was considered to be variable, meaning that natural membrane frequencies could be modulated. All the relevant membrane characteristics are displayed hereinafter. In addition to the introduction of flexible membranes, a forced-oscillation system was developed so as to analyze unstable mechanism behavior when inhibitor oscillation is forced and controlled. The rigid inhibitor was then coupled to a motor in order to provide regular oscillation motion with a 2.5 deg angle at frequencies ranging from 0 to 360 Hz (cf. Figure 1). A high-speed brushless motor and polyflex 3M belt provided a 0.106 Nm couple, which was found to be strong enough to provide the inhibitor with an oscillating motion.

To characterize the flowfield, mean and fluctuating-pressure signals were measured at the head end by a flush-mounted piezoelectric quartz transducer with an accuracy rate of 10 and 0.02 Pa for static and fluctuating pressure, respectively. The velocity signals were recorded from a 5 μm single miniature probe for spectral analyses and from a 5 μm X miniature probe for mean characterization; estimation of errors for the mean and fluctuating data was found to be equal to ± 1 and $\pm 2.5\%$, respectively, and mass flow rate measurement accuracy registered at $\pm 2\%$. Pressure and velocity signals were recorded by a 12-bit A/D board and sampling frequency was set equal to 10 kHz, and the maximum spectral frequency was found to be lower than 1000 Hz. fast Fourier transform algorithm was used to estimate spectral answers constructed by a 50 averages of 4096 points with a resolution frequency of 2.44 Hz. To assess correlation coefficients between fluctuating signals, finite inverse Fourier transform was used. Phase-averaged quantities were obtained by averaging the instantaneous velocities in one single period corresponding to the main excited frequency found in the spectral distribution. The period was subdivided into 80 time intervals, and phase-averaged data were processed through 2500 cycles. Considerable effort went into ensuring the accuracy of the data, and the phase-averaged focus facilitated qualitative insights into the vortex-shedding mechanisms.

III. Forced-Inhibitor Oscillations

Before any investigation of fluid/structure influence, the initial step consists of identifying how mechanisms arise in the SRM framework; in our experiment, this was intensively performed from a cold-gas setup [11–13]. During a SRM firing life, specific time delays are pinpointed when oscillations amplify; the MICAT experimental setup facilitates depiction of the main unstable mechanisms during these critical periods. Even though the midcombustion time step does not yield the highest oscillating-energy rate, the two vortex-shedding mechanisms (shear-layer vortex shedding and wall vortex shedding) strongly interact, and it is possible to depict a fluid/structure role in such interactions. To succinctly present unstable mechanism behavior, Fig. 2 shows the change in power spectral densities of pressure and velocity fluctuations versus the internal Mach number ranging from 0.06 to 0.11. The fluctuating properties of pressure and velocity were recorded at strategic locations, with the head end serving as the reference location for pressure and velocity fluctuations, which were recorded in the inhibitor's wake and also in the rear end of the chamber close to the injecting wall. Pressure fluctuations (Fig. 2) are characterized mainly by a concentration of energy around the first longitudinal acoustic mode of the chamber ($f_{1L} \sim 280$ Hz) for $0.06 \leq M \leq 0.11$. In this specific Mach number range, it is possible to follow several linear evolutions of the highest excited peak at frequencies that are punctuated by jumps lowering the dominant frequency peak. In addition, pressure fluctuation activity clearly highlights the significant increase of energy for $0.08 \leq M \leq 0.09$, thereby underlining resonance in that specific range. For higher

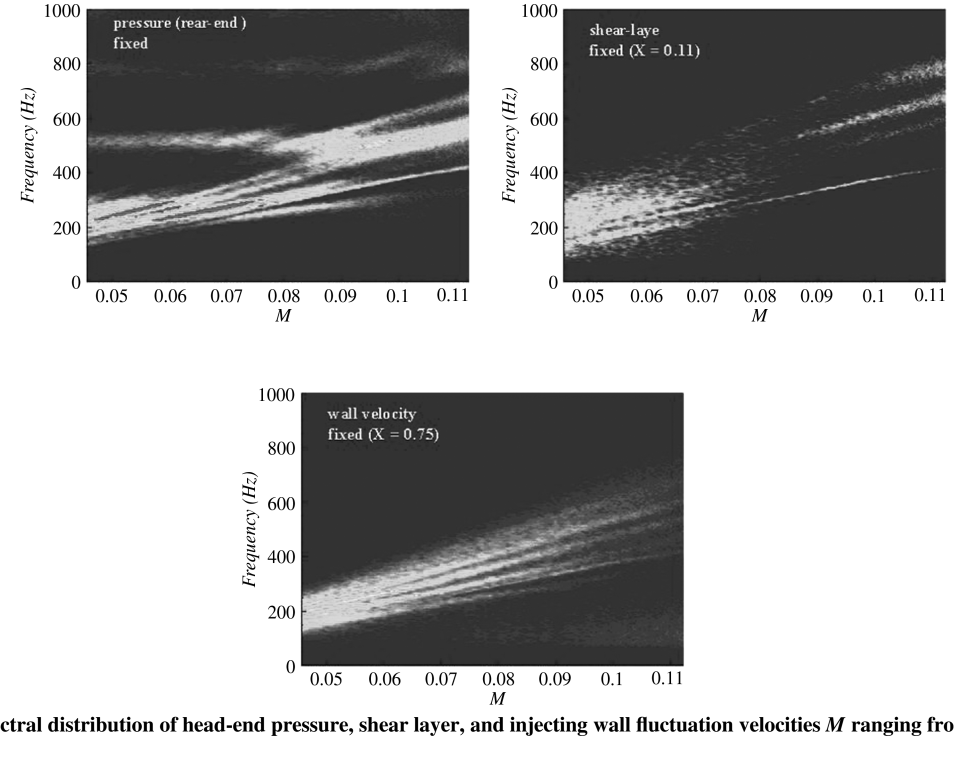

Fig. 2 Power spectral distribution of head-end pressure, shear layer, and injecting wall fluctuation velocities M ranging from $M = 0.06$ to 0.14.

Mach numbers ($M \geq 0.11$), concentration of energy is not so significantly pronounced; rather, it occurs in the vicinity of f_{2L}. In addition to frequencies close to f_{2L}, the Mach number increase produces an amplification of some frequency peaks that also evolve linearly with Mach number. Continuous linear heightening is likewise detected from f_{1L} for $M \geq 0.11$ as though the two mechanisms were interacting with each other. Figure 2 shows a similar pseudo-3-D plot highlighting the characteristic shear-layer frequency change with Mach number. Spectral organization is obviously not specifically centered around a single frequency in the shear layer. One may nonetheless observe some scattered frequency peaks that evolve more or less linearly along with Mach number. For $M \geq 0.11$ shear-layer behavior is driven mainly by two trends: i.e., linear change of a peak close to f_{1L} and energy concentration close to f_{2L}. In the rear end of the chamber close to the injecting wall, spectral fluctuating activity is marked by three distinguishable linear evolutions in frequency for $M < 0.11$, whereas for higher Mach numbers, the change is not so emphatically pronounced. To explain the mechanisms arising in such cases, it is important to bear in mind that vorticity concentration close to injecting walls is dynamically driven; i.e., the characteristic frequency evolves linearly along with convective velocity. Thus, when Mach number goes up, the frequency of the wall vortex-shedding phenomenon is likewise augmented, and as soon as the involved frequency narrows f_{1L} ($0.08 \leq M \leq 0.10$), acoustic waves are enhanced on that specific frequency. The shear layer is then strengthened through alignment on the frequency and, as a result, a resonance phenomenon arises. However, the shear layer is still significantly stressed and the resonance mechanism is not strong enough to deeply modify its behavior. For higher Mach number levels, the frequencies involved in the wall-injection phenomenon similarly increase up to f_{2L} for $M \sim 0.12$; acoustic waves generated from the impingement of vortices upon the rear end of the chamber strengthen and affect the shear-layer development by introducing vortex shedding at frequencies close to f_{2L}. It is obvious from spectral analysis that a pairing phenomenon occurs and explains the existence of a single frequency close to f_{1L} in the shear layer (Fig. 2). As is clearly noted in cases of spectral analysis, pressure/velocity interactions may be significant, and yet the attendant mechanisms are not completely interlocked. The complex mechanisms have been studied and analyzed in detail [11]. Computing the spatiotemporal correlation coefficient between pressure and velocity is likely to shed light, for instance, on the interactions that help to amplify instability in SRMs. It is interesting to study how these interactions and couplings are sensitive with regard to inhibitor oscillations.

As stated in the Introduction, such sensitivity was first studied with a forced-oscillation setup. Effects of a forced-oscillation inhibitor were analyzed with a 2.5 deg tilted-angle amplitude, and its frequency was considered as variable. Figure 3 shows the head-end pressure fluctuation responses at several forced frequencies for $M = 0.095$. This figure was chosen because it corresponds to a Mach number for which resonance arises. To more clearly highlight the changes between fixed and forced-oscillation inhibitors, each spectral answer obtained with a movable inhibitor has been superimposed to the one obtained with the rigid inhibitor. From these spectral answers, it is obvious that the forced oscillating motion of the inhibitor plays a significant role in pressure-fluctuating behavior. For $f_F = 100$ Hz spectral activity in the pressure field is strengthened at the f_{1L} first acoustic mode, and a low-energy peak is identified at the imposed frequency. This trend is amplified for $f_F = 150$ Hz; actually, the peak at that frequency is significantly amplified, whereas the amplitude of the main peak at f_{1L} is reduced. The forced frequency becomes the dominant one for $f_F = 200$ Hz, and the energy involved around f_{1L} is no longer modified. As soon as the forced frequency aligns with f_{1L} a single peak takes shape and is significantly amplified with regard to the fixed-inhibitor configuration. Figure 4 plots spectral density behavior in the shear layer for the similar f_F forced-oscillation frequencies. As expected, shear-layer characteristic spectral density is composed of many peaks loosely organized around one dominant frequency close to f_{1L}. This finding confirms the fact that shear-layer development is turbulent, and the acoustic mode interacts in ways favoring its specific frequency. The forced oscillating motion of the inhibitor at $f_F = 100$ Hz does not yield vortices at that frequency, and the main vortex-shedding frequency close to 280 Hz is strengthened. This is not the case for $f_F = 150$ Hz and $f_F = 200$ Hz, in which the shear layer is organized around the forced frequencies. The flapping motion is strong enough to compel the shear layer to align at the latter. In addition, spectral distribution highlights a duality between the aeroacoustic coupling and the forced oscillation of the inhibitor that superimposes vortex-shedding frequency at its own frequency.

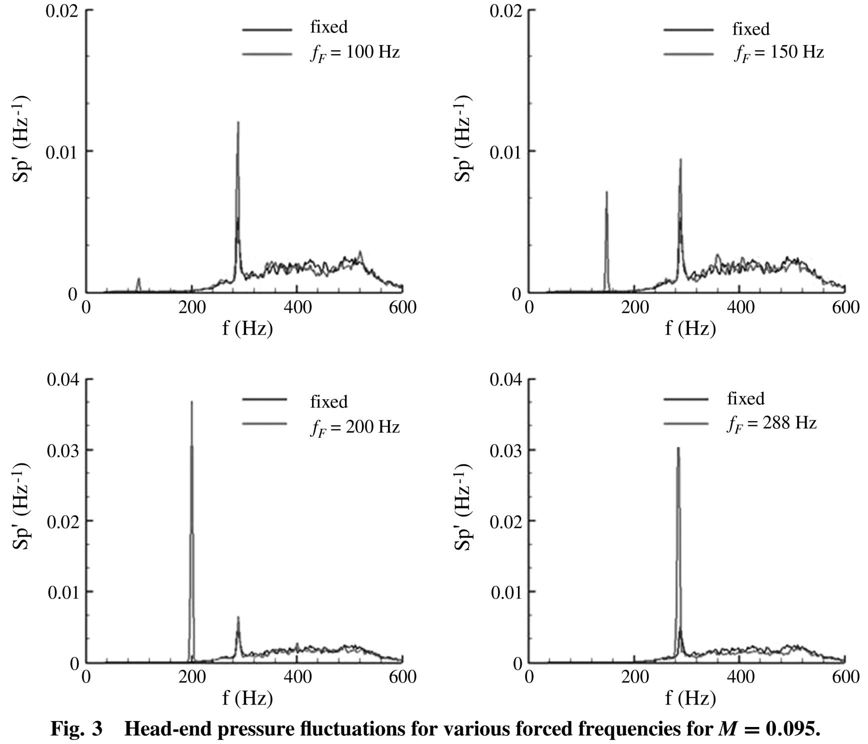

Fig. 3 Head-end pressure fluctuations for various forced frequencies for $M = 0.095$.

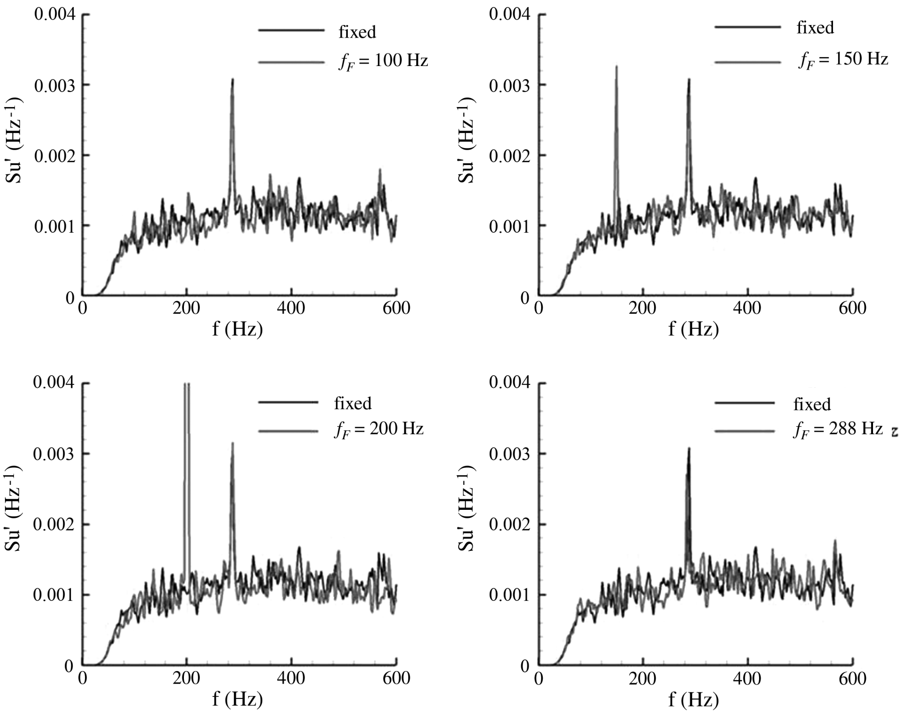

Fig. 4 VSO spectral activity for various forced frequencies for $M = 0.095$.

It nonetheless remains surprising that for $f_F = f_{1L}$ the shear layer is not affected; i.e., a peak is observed at that frequency, but no amplification occurs and the spectral answer is similar to the one observed under fixed conditions. One might expect that the forced motion at the frequency of the shear layer would be amplified and strengthen the vortex shedding, but this not the case. And so, in order to more accurately depict forced motion impact, we closely studied spectral organization close to injecting walls, and similar observations of forced inhibitor influence on the fluctuating activity of velocity close to the injecting walls may be put forward (not shown), and a similar conclusion may be put forward. With this in mind, temporal correlations were computed and two kinds of correlation profiles are shown (Fig. 5). First, we focus on the ability of wall vortex shedding to generate an acoustic wave; in order to do this, $R_{u'p'}$ correlations between velocity fluctuations recorded in the rear end of the chamber close to the injecting wall and head-end fluctuating pressure were evaluated with the inhibitor under forced conditions. For the reference case, i.e., under fixed conditions, a significant peak for τ^+ is clearly observed with maximum levels higher than 20%. According to its definition, a maximum peak at a positive time delay means that a wall vortex is first detected by the hot wire before the information (a wall vortex structure is developing) is transformed somewhat later into pressure recorded at the head end. The wall vortices are coherent enough to generate a pressure wave when structures impinge upon the submerged nozzle and the pressure wave travels up to the head end. No significant correlation peak is observed for negative time delay: i.e., no feedback loop occurs; this explicitly indicates that the wall vortex-shedding mechanism is not acoustic-dependent; rather, it tends to be involved through dynamic phenomena. As clearly demonstrated by Staab and Kassoy [15], wall vortex-shedding mechanisms are induced by interaction between core flow and injecting wall; i.e., they are dynamically dependent. When the inhibitor oscillates at $f_F = 100$ and 288 Hz, no significant change is observed in the $R_{u'p'}$ profile compared with the change obtained in the reference case; peak level is more or less unaltered. In addition, levels of $R_{u'p'}$ along time delays are amplified, except when peaks arise, for all f_F. According to Vetel et al. [13], such amplification can be explained by superimposition of several cycles of the coupling phenomenon. It also appears fundamental to underline that the frequency at which the inhibitor oscillates may interact on the wall vortex-shedding phenomenon. Actually, at $f_F = 200$ Hz the $R_{u'p'}$ profile exhibits levels of correlation that have significantly increased; for instance, the peak at τ^+ reaches 36%, and the modulating levels are higher than 10%. For $f_F = f_{1L}$, the $R_{u'p'}$ profile is somewhat similar to the one obtained at $f_F = 100$ Hz, for instance.

To explain why such amplification arises for $f_F = 200$ Hz, cross-correlations were computed (not shown) between velocity signals recorded at the origin of the shear-layer development and in the rear end of the chamber close to the injecting wall. Although almost no significant levels of correlation were detected for the reference case and for $f_F = 100$ and 288 Hz, significant correlations close to 10% are exhibited for $f_F = 200$ Hz. Shear-layer and wall-injection correlations underscore a close correlation between the shear-layer and wall vortex-shedding mechanisms. For dynamic conditions and the forced-oscillation-inhibitor frequency, the shear layer directly triggers the wall vortex-shedding mechanism, and this constitutes one of the main results of analysis: a perturbing shear layer through forced oscillation of the inhibitor may directly impact the development of wall vortex shedding. This quite explicitly means that fluid/structure coupling directly interacts on the second source of instability in a SRM: i.e., wall vortex shedding. It should nonetheless be borne in mind that introducing a forced oscillating motion strongly modifies whole flowfield behavior at a level that is by no means comparable with changes that may occur in the case of a flexible inhibitor. In fact, the energy brought into play with a flexible inhibitor and a forced-oscillation inhibitor is most likely not comparable at all. Does such potential fluid/structure coupling impinge upon the level of instability observed and/or on vortex-shedding mechanisms?

IV. Flexible Membrane and Its Role in an Unstable Process

Fluid/structure and its relationship with regard to unstable development is a highly complex task that needs to be addressed. In the case of a flexible membrane, numerical simulations remain difficult to achieve and are also expensive in terms of CPU time. In addition, further experimental investigations are necessary in order to fully investigate the potentialities of flexible membranes [10,16]. As far as we know, no experimental setup has comprehensively analyzed fluid/structure coupling with SRM configuration; the presence of

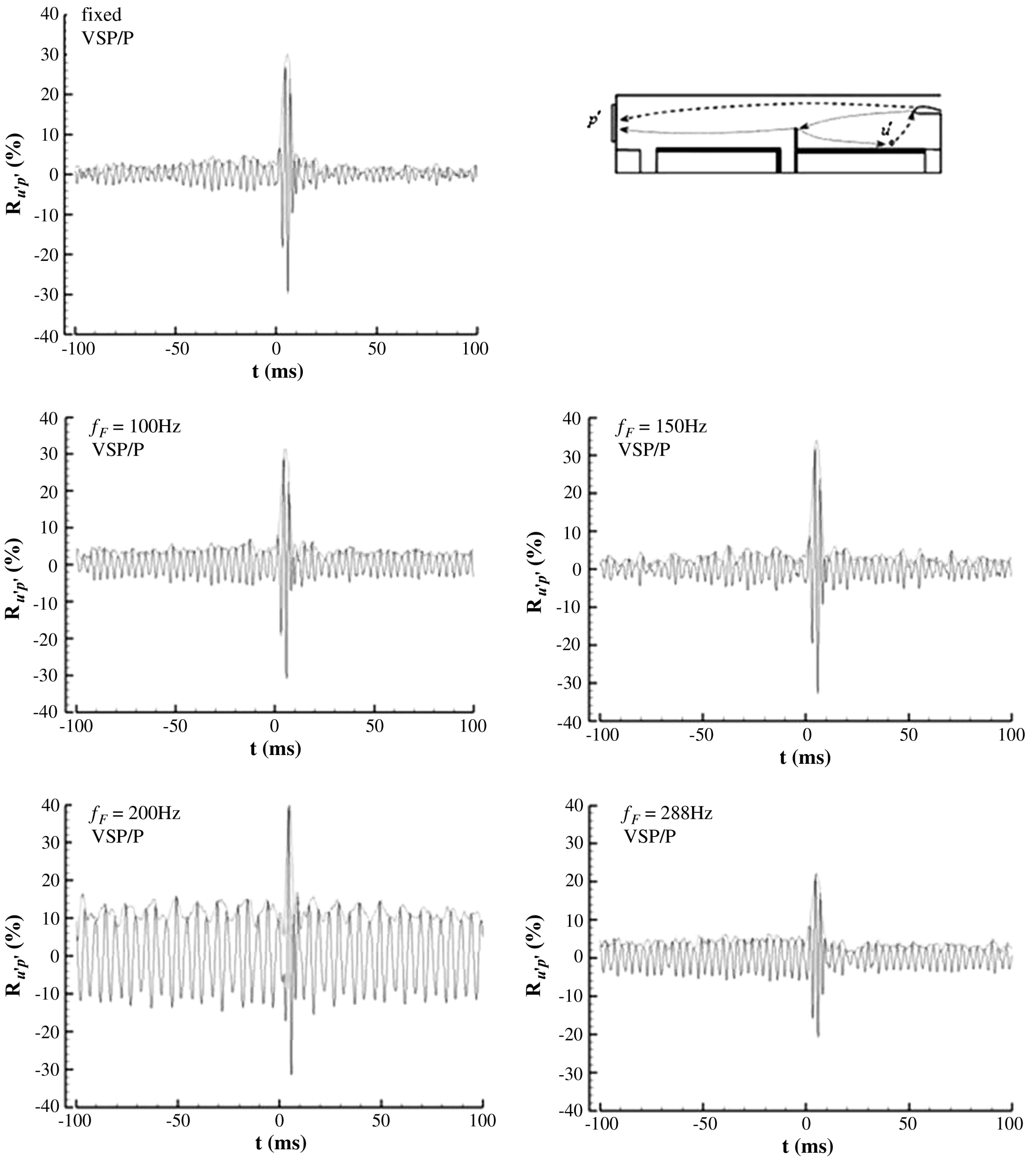

Fig. 5 $R_{u'p'}$ **correlations between velocity fluctuations recorded in the rear end of the chamber close to the injecting wall and head-end fluctuating pressure for several forced inhibitor conditions.**

wall injection underscores unstable mechanisms such as the wall vortex-shedding phenomenon. For now, we will focus on the potential effects of flexible membranes by replacing a rigid membrane with several membrane thicknesses ranging from $0.5 \leq \varepsilon \leq 1.0$ in order to modulate its natural frequency. Table 1 lists the estimated mode of each membrane thickness from numerical finite element analysis. The frequency range extends from 265 to 470 Hz for thickness $0.5 \leq \varepsilon \leq 1.0$.

The first step consists of estimating the potential effect of a flexible inhibitor in the existing setup by comparing the levels of $\sqrt{\bar{P}'^2}/P$ recorded at the head end. Figure 6 shows the $\sqrt{\bar{P}'^2}/P$ levels reached with regard to Mach number for several flexible inhibitors; the data are compared with those obtained for the fixed inhibitor: i.e., the reference case. Two trends are exhibited. For $M \leq 0.11$, fluctuating levels are amplified for all ε; for instance, at $M = 0.09$, fluctuating levels are increased by 9.1, 12.2 and even 12.7% of the level reached under fixed conditions for $\varepsilon = 0.5$, 0.7, and 0.9, respectively. We should then recall that under such dynamic conditions a weak coupling arises close to f_{1L}. For $M > 0.1$, a transition from f_{1L} to f_{2L} longitudinal mode occurs for the fixed-condition fluctuating levels; these levels are of the same order of magnitude for $\varepsilon = 0.7$ and 0.9 as those reached for the fixed condition. However, for $\varepsilon = 0.5$ a significant pressure-fluctuating decrease is observed; such a decrease is equal to 12.1% and even 14.3% for $M = 0.12$ and 0.13, respectively. Although all the flexible inhibitors studied (except $\varepsilon = 0.5$) provide similar pressure-fluctuating levels for $M > 0.11$, there is a surprising decrease just for $\varepsilon = 0.5$. How are we to interpret such results?

Table 1 Natural mode estimation regarding the material and the ε thickness considered

ε	Natural mode, Hz	Material
1 (rigid condition)	6510.	Aluminium
0.5	265.	33% acrylonitrile
0.6	316	Nitrilic
0.7	334	Nitrilic
0.8	354	Nitrilic
0.9	377	Nitrilic
1.0	407	Nitrilic

We should not forget that inhibitor inclination can be responsible for significant changes in pressure-fluctuating levels. Vetel et al. [17] compared internal acoustic response of small-scale SRM and cold-gas setup; they investigated inhibitor shape influence, with each factor leading to specific pressure oscillation behavior. The case of a

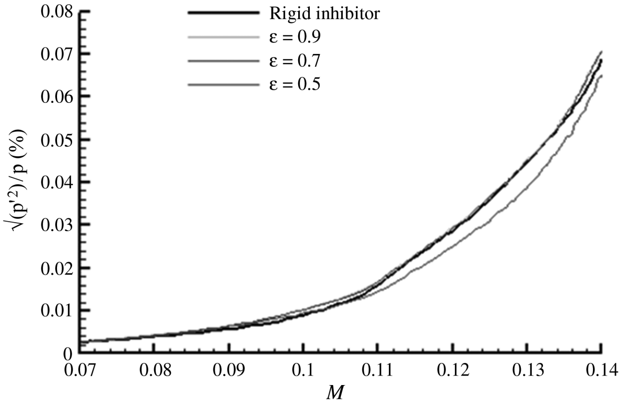

Fig. 6 Change of $\sqrt{P'^2}/P$ with regard to Mach number for various flexible inhibitors.

strong bent shape inhibitor was also analyzed and the data clearly show significant pressure level modification with regard to a straight inhibitor case. The inhibitor inclination was fixed equal to 60–70 deg with regard to the vertical; i.e., the inhibitor was located very close to injecting walls. This surely explains why pressure levels were significantly altered: i.e., vortex shedding that develops in the obstacle wake is literally forced to lean up against the injecting wall; consequently, drastic changes in between the vortex-shedding phenomena are to be expected, along with wall-injection vortex shedding. As for a flexible inhibitor, it may be bent due to the flowfield load with lower tilted angle. Numerical analysis was initially carried out so as to roughly estimate inhibitor deviation with ANSYS mechanical software, which allows for determination of the stationary inhibitor tilted-angle position under flow load. It is extremely important to note that we performed such analysis only so as to qualitatively estimate the tilted angle; it was with this objective in mind that we took into consideration a uniform loading. Table 2 lists the angles estimated numerically for various ε levels, as well as estimated values from experimental views. The experimental estimation of the tilted angle was obtained from a picture of the inhibitor during the flowfield test (Fig. 7); it is clear that angle levels estimated from the numerical tool are of the order of magnitude of what is experimentally observed with a maximum deviated angle of 25 deg. At this point, one fundamental question remains. Is a tilted angle of 25 deg strong enough to interact on whole flowfield development, or does a fluid/structure coupling occur and literally induce significant oscillation motion in the inhibitor?

To answer such a question, experimental tests were carried out with a rigid but bent inhibitor, and the deviation angle was chosen to be equal to the angle observed with flexible inhibitors: i.e., with a maximum of 25 deg. As the bent inhibitor was made of steel, it prevents any oscillating motion and may be considered as fixed. The pressure-fluctuating amplitudes obtained for both straight and bent rigid inhibitors (not shown) are strictly similar in the whole Mach number range studied. This finding explicitly demonstrates that not only is the flexible inhibitor bent, but also that actual fluid/structure coupling is initiated and that a self-sustained oscillation of the inhibitor occurs. As pressure fluctuations are modified under such conditions, the oscillating inhibitor motion alters the unstable mechanism: i.e., the vortex-shedding phenomena arising in a SRM chamber. A second step consists of depicting how the oscillating motion of the flexible inhibitor modifies unstable processes. Changes in the vortex-shedding phenomena arising in the obstacle‘s wake are expected, but analysis of forced oscillation has clearly shown that wall vortex shedding may be significantly altered as well. Because of the existence of two different trends with regard to Mach number, it is necessary to analyze spectral responses in the head-end pressure signals for various flexible-inhibitor thicknesses.

Table 2 Deviation angle of the flexible inhibitor for $M = 0.095$

ε	Angle of deviation, deg	Material
1 (rigid condition)	0	Aluminium
0.5	16	Nitrilic
0.6	9	Nitrilic
0.7	6.4	Nitrilic
0.8	5.0	Nitrilic
0.9	3.8	Nitrilic
1.0	2.6	Nitrilic

Figure 8 displays the pseudo-3-D spectral answers for $\varepsilon = 0.5$, 0.7, and 0.9 for the complete Mach number range ($0.06 \leq M \leq 0.14$), and distribution for the reference case (straight and rigid inhibitor) has also been plotted to render comparisons easier. For $M \leq 0.11$, energy contained in the 200–300 Hz frequency band appears to be less concentrated around a single frequency, at least for $\varepsilon = 0.9$ and $0.06 \leq M \leq 0.11$ and for $\varepsilon = 0.7$ and 0.5, but only for $M < 0.09$ approximately. In these two cases, energy concentration around a single frequency is clearly observed for $0.092 \leq M \leq 0.14$ and $0.09 \leq M \leq 0.13$ for $\varepsilon = 0.7$ and 0.5, respectively. This concentration amplification does not occur for the reference case and seems to be responsible for a pressure fluctuation increase in that Reynolds range. For $M \geq 0.11$, the split between first and second acoustic modes occurs for all ε, but at the same time, the smaller ε the more the frequency change around f_{2L} is organized. Even if such a trend is not so clearly pronounced, it should be recognized that linear evolution of the highest-energy frequency punctuated by a frequency jump is detected, at least for $\varepsilon = 0.9$. In addition, energy concentrates significantly around a single frequency for $\varepsilon = 0.5$ and $M \geq 0.12$. The next step consists of pinpointing the mechanisms that are amplified and/or altered with regard to the introduction of a flexible inhibitor. We have decided to focus on the $\varepsilon = 0.5$ case because it behaves similarly to the other inhibitor studied for $M \leq 0.11$ and is the only case that yields a significant pressure fluctuation reduction for $M > 0.11$.

In the low Mach number range studied ($M = 0.095$), average velocity and fluctuating activity were analyzed and compared with the dynamic field obtained for the reference case: i.e., for a fixed condition. Figure 9 presents the velocity profile of the mean longitudinal component at several axial locations for $M = 0.095$ and it is obvious that introduction of a flexible inhibitor significantly modifies average mean velocity distribution. Actually, in the immediate vicinity of the longitudinal inhibitor location, velocity profiles in the inhibitor location are not as significantly stressed as under fixed conditions; for $0.0 \leq X \leq 0.46$, it is clear that gradients on velocity profiles are not as significant. As shown in Fig. 8, flexible inhibitors are bent under flowfield loading that significantly reduced shear flow intensity. Note that for $X > 0.46$, velocity profiles are similar for all inhibitors studied. In the same figure, the I_T turbulence intensity profiles are also plotted for the same longitudinal axial location and the fluctuating activity is likewise sensitive to the nature of the inhibitor. Just in back of the inhibitor location, I_T profile is characterized mainly by a peak corresponding to local maximum turbulent activity; the latter is smaller in intensity and less vertically located for $\varepsilon = 0.5$ than for the fixed case. At the origin of the shear layer, the I_T maximum level reaches 22%, a level that decreases slightly up to 19% at $X \sim 0.46$. Then turbulence intensity I_T is amplified to reach levels higher than 30% in the rear part of the chamber. This increase corresponds to the wall vortex-shedding contribution. Although the maximum peak of I_T is decayed toward the upper wall for a fixed condition, the opposite occurs for $\varepsilon = 0.5$; i.e., the maximum peak is located close to the injecting wall for $X \leq 0.54$. For $X > 0.54$, I_T profiles tend to become more or less similar in shape for the two different kinds of inhibitors studied but the levels for $\varepsilon = 0.5$ are invariably smaller than those involved under the reference case. Being flexible, the inhibitor is bent, thereby providing smaller shear stress in the shear layer and lower fluctuating activity. Under rigid conditions, the shear layer is mainly upward-oriented, whereas the opposite occurs under flexible conditions: i.e., vortices arising in the inhibitor's wake are convected toward the injecting walls. In addition, as shown above, the flexible inhibitor offers an oscillating motion that may help to force energy to

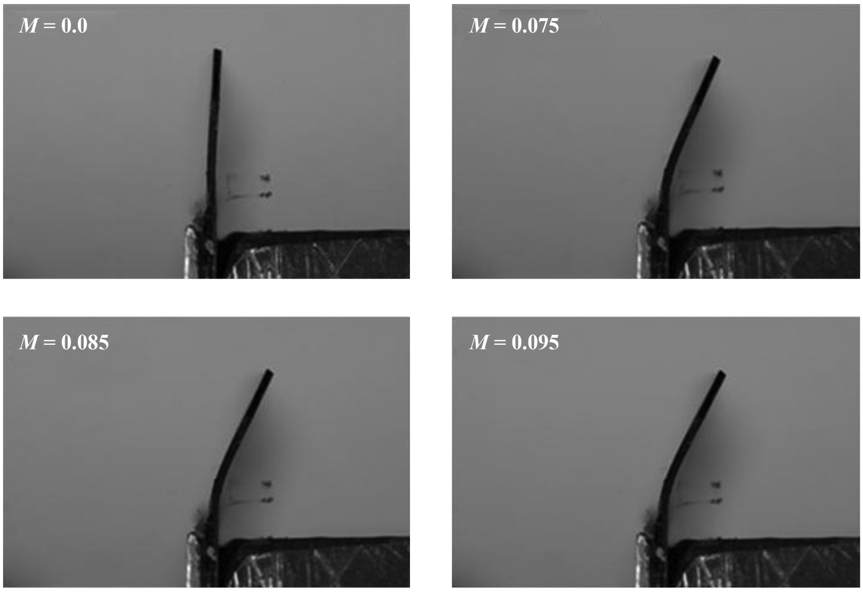

Fig. 7 Views of inhibitors under flowfield loading for $\varepsilon = 0.5$, 0.7, and 0.9.

concentrate around a specified frequency. To highlight this potentiality, Fig. 10 presents the spectral distribution of the fluctuating activity in the shear-layer development quite close to the inhibitor location (at $X = 0.035$); it is obvious from the spectral distribution that a flexible inhibitor favors a single frequency and that spectral distribution is characterized mainly by a single peak that emerges at approximately 285 Hz; around 90% of the whole energy is contained in a 270–300 Hz frequency band. Considering the material of which the inhibitor is formed, its natural frequency was estimated at roughly 265 Hz (i.e., a real coupling between flexible inhibitor and flowfield consequently occurs); it may as a result directly force fluctuating energy to concentrate around a single frequency. Although overall levels are reduced, energy is significantly organized around the one frequency. To estimate how vortex shedding from obstacles (VSO) and vortex shedding arising from the injecting walls [vortex shedding parietal (VSP)] are modified, Fig. 11 shows the $R_{u'p'}(\tau)$ obtained for VSP/pressure correlation; the two time delays at τ^+ and τ^- are significantly amplified, with levels equal to 12.9 and 15.7%, respectively, and peak intensities reach d 5.2 and 12.7% under the fixed configuration. The increase of τ^+ is significant between fixed and flexible inhibitors. This means that the coherence of vortex structures developing at the origin of the shear layer is enhanced with flexible inhibitor and consequently helps to generate stronger pressure waves while impinging upon the rear end of the chamber. A similar trend is detected in the $R_{u'p'}(\tau)$ coefficients between VSP and pressure, with a τ^+ peak increase higher than 40% between the fixed and the flexible inhibitor. The VSP phenomenon is a mechanism that significantly contributes to pressure wave generation. The correlation at τ^- is also significantly amplified; i.e., pressure waves contribute to wall vortex-shedding enhancement. At first glance, such a finding seems to be opposed to the nature of wall vortex-shedding mechanism itself: i.e., the latter being derived from a natural dynamic instability phenomenon. To better understand how a flowfield organizes, it would be of interest to depict how structures behave. However, experimental conditions do not allow for direct investigation of a flowfield from optical measurement, with the

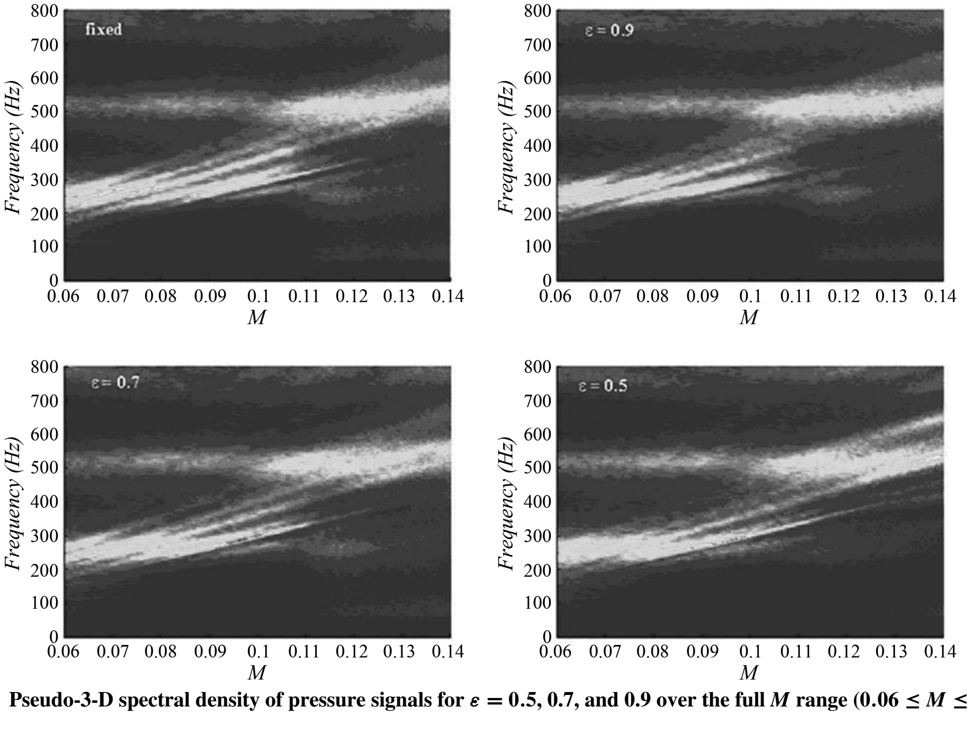

Fig. 8 Pseudo-3-D spectral density of pressure signals for $\varepsilon = 0.5$, 0.7, and 0.9 over the full M range ($0.06 \leq M \leq 0.14$).

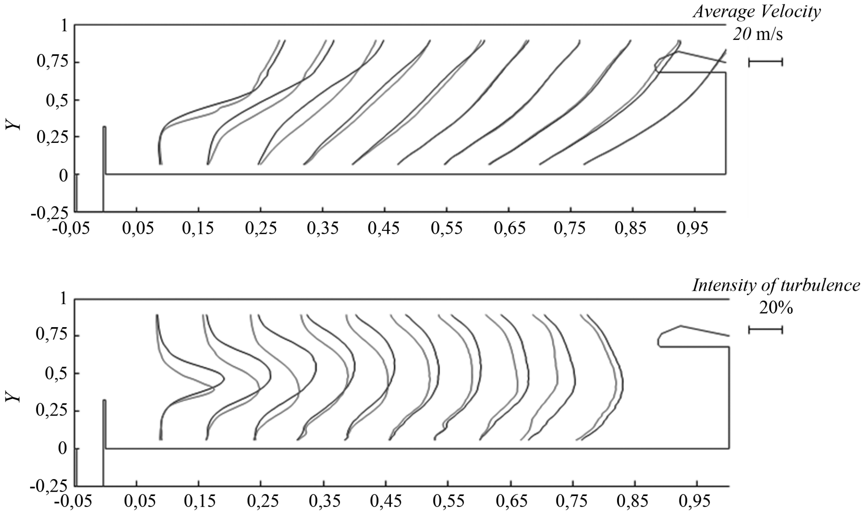

Fig. 9 Velocity of the mean longitudinal component and turbulence intensity profiles at several axial locations for $M = 0.095$.

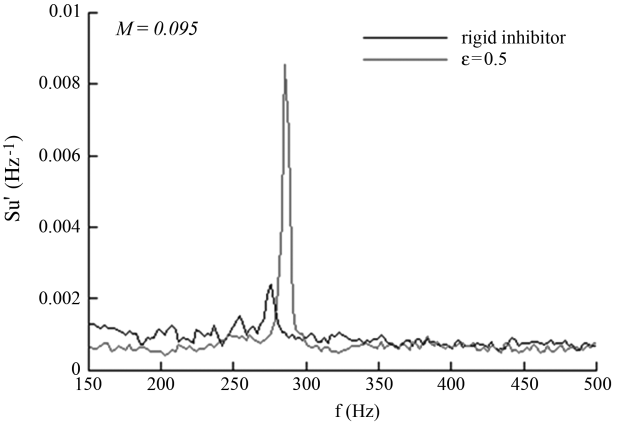

Fig. 10 Spectral distribution of the fluctuating activity in the shear-layer development in close proximity to the inhibitor location (at $X = 0.035$).

injecting wall material impeding any flow-seeding. Thus, to qualitatively observe structures, we employ a phase-averaged method already successfully used to visualize the end-of-combustion configuration [13]. In that case, however, a resonant phenomenon arises, forcing pressure and velocity signals to organize mainly around a single frequency, as is not the case in the present configuration, where a wide range of frequencies enter into play. That said, phase-averaged technique effectively helps to qualitatively depict structure organization, which was carried out with phase-averaged lock frequency at the highest excited frequency contained in the pressure signal. As a consequence, even if it may somewhat alter the averaging procedure, it does provide an opportunity to portray structure behavior back to the obstacle location (Fig. 12). Phase-averaged longitudinal and transverse velocities were first obtained as a function of time and location, and pressure signals from the head end served as the reference signal. The rotational component was then obtained via Taylor's hypothesis. The time t and vorticity were nondimensionalized by the period T and the frequency of the

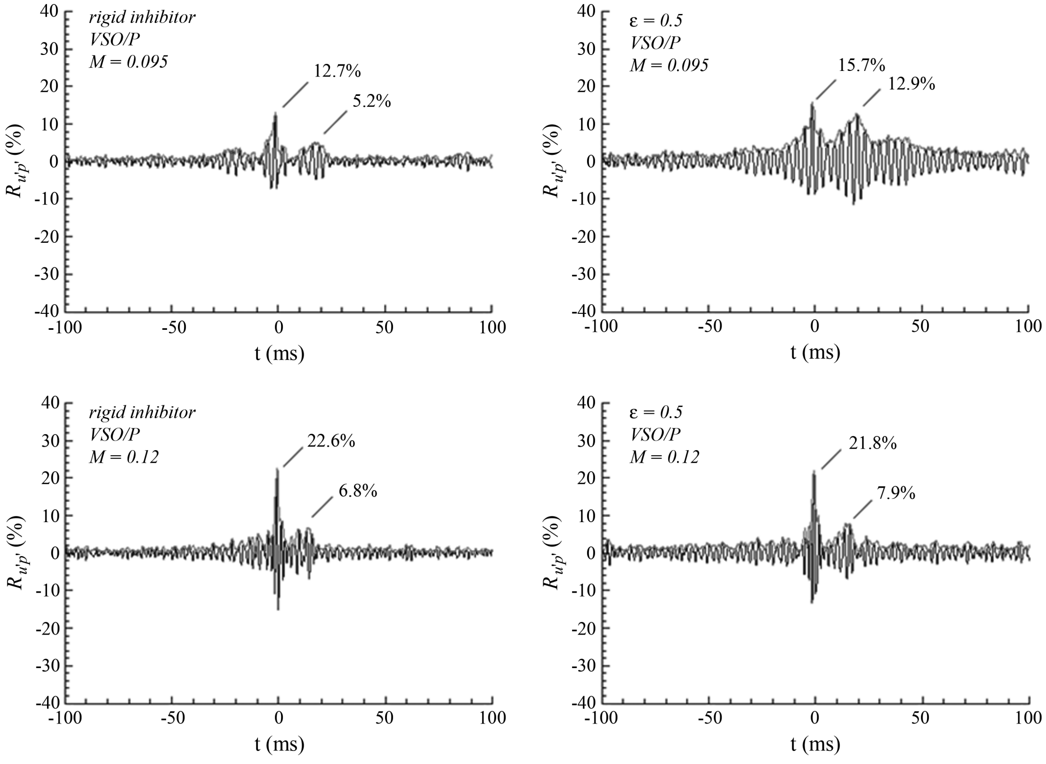

Fig. 11 $R_{u'p'}(\tau)$ obtained for VSP/pressure correlation.

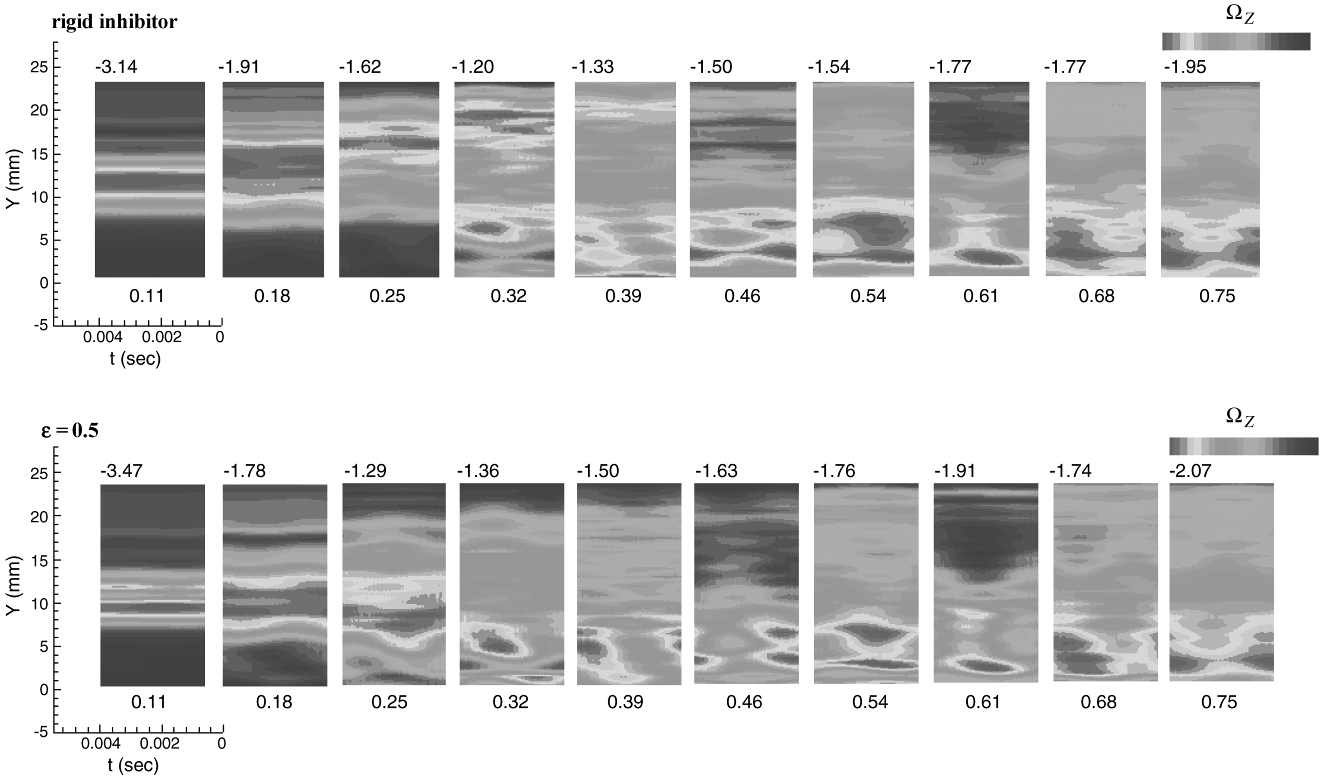

Fig. 12 Phase-averaged estimation of the z-vorticity component.

phenomenon, respectively. Directly in the wake of the inhibitor, the shear layer is expelled upward for the fixed-inhibitor case and the z-vorticity component is rapidly dissipated, confirming lateral shear-layer expansion. At $X = 0.39$, one can detect some vorticity development in the vicinity of the injecting wall and from that location, it is obvious that the wall and main flow interact, resulting in wall vorticity generation. For $\varepsilon = 0.5$, everything occurs as though the flowfield were more coherently organized; vortex structures are initiated in the obstacle wake and the structure path is oriented mainly toward the injecting wall. Structures lean up against the injecting wall and strengthen from injecting conditions. Thus, considering all the qualitative and quantitative data obtained, it is obvious that introducing a flexible inhibitor induces the flowfield to behave in a laminar way. At the very least, even if turbulent dissipation still occurs, it serves to underscore structure coherence. Such a relaminarization trend occurs due to shear intensity reduction and because the dynamic paths of the structures are modified, which enhances VSO/VSP interaction.

It is now time to address the role of flexible thickness in the whole unstable process. In other words, does the natural frequency of the flexible obstacle play a role in unstable process development? The answer seems to be negative, at least in the lower Mach number range studied. Actually, natural frequency varies significantly with ε as listed in Table 1; for instance, the latter is assumed to be equal to 205 Hz for $\varepsilon = 0.5$, whereas it reaches 340 and 377 Hz for $\varepsilon = 0.7$ and 0.9, respectively. Moreover, the levels of fluctuating pressure at the head end are globally of the same order of magnitude for all ε, at least for the lower Mach number range studied: i.e., $M \leq 0.11$. However, in regard to the spectral answers of head-end pressure for fixed and flexible inhibitors ($\varepsilon = 0.5$, 0.7, and 0.9) in Fig. 10 for $M = 0.095$, it is obvious that the latter is integrally linked to the nature of the inhibitor tested. For instance, $\varepsilon = 0.5$ and 0.7 highlight energy concentration close to 280 Hz, whereas under the same dynamic conditions, the spectral answer provided by a fixed inhibitor is larger. Note that a similar trend is likewise detected for $\varepsilon = 0.9$. Taking into account the roughly estimated natural frequency, potential oscillating motions of inhibitor literally impact in the shear-layer development from an unsteady point of view, forcing the latter to organize around a single frequency. In addition, the more the natural frequency is close to frequencies at which the shear layer develops, the easier it is to alter shear-layer development; that is why significant changes occur for $\varepsilon = 0.5$ and 0.7 in the pressure spectral answer. As expected, fluid/structure interaction is strong enough to interact and modify shear-layer response, reinforcing the shear layer at a single frequency. As a consequence, vortex-shedding coherence is enhanced and due to a modified convection path, vortex shedding from the shear layer from injecting wall conditions is rendered evident. An increase in unstable process level consequently occurs. For $M > 0.11$ and $\varepsilon = 0.5$, the flexible membrane preferably highlights the flowfield close to the first longitudinal mode and thus delays the transition from f_{1L} to f_{2L}. As a consequence, VSP/VSP interaction is altered, yielding an overall diminution of fluctuating level.

V. Conclusions

Fluid/structure coupling effects in the framework of SRM instability have been analyzed from the dedicated MICAT cold-gas subscale model. This is the first time fluid/structure coupling has been studied experimentally to depict its potential influence in segmented propellant motors. One means of analyzing fluid/structure influence was studied by replacing the rigid inhibitor with a flexible one. Its own mode was modulated from 260 to 400 Hz by altering membrane thickness. We have focused mainly on the effect of the flexible membrane under turbulent flowfield conditions. The first self-sustained oscillations of the membrane were identified. The changes observed in the shear layer and wall-injection vortex-shedding mechanisms are not due to a static deformation, but to a real coupling between the inhibitor and the whole flowfield development. For the lower Mach number range studied ($M < 0.11$), the introduction of a flexible membrane favors the flow's organization around a single frequency in the shear layer; i.e., a laminarization process occurs. Despite the fact that the overall levels in the velocity fluctuations are weaker than those obtained in the rigid inhibitor configuration, vortex coherence is strengthened, resulting in heightened overall fluctuating-pressure activity. For $M > 0.11$, the flexible membrane does not play a role anymore, except for the $\varepsilon = 0.5$ thickness. Under such conditions, the flow is mainly organized around f_{2L}, and the $\varepsilon = 0.5$ membrane favors a frequency close to the first longitudinal acoustic mode. It then delays then the f_{1L} to f_{2L} transition and contributes to the significant pressure oscillation decrease.

This work is but a first step in the long process of controlling instability mechanisms in SRMs, and the findings clearly demonstrate that the inhibitor membrane exerts a significant impact. Its material characteristics should be taken into consideration. A next step will be to depict its influence when resonance is clearly locked. Actually, internal geometry change during firing exerts a major influence in the resonance mechanism and *end-of-combustion* time steps correspond to an increase in pressure oscillations, which is integrally linked to the alignment between the two vortex-shedding mechanisms (back to the obstacle and along the injecting walls). It would be interesting to see whether or not inhibitor flapping is strong enough to interact when such resonance occurs.

References

[1] Dotson, K. W., Koshigoe, S., and Pace, K. K., "Vortex-Shedding in a Large Solid Rocket Motor Without Inhibitors at the Segment Interface," *Journal of Propulsion and Power*, Vol. 13, No. 2, 1997, pp. 197–206. doi:10.2514/2.5170

[2] Scippa, S., Pascal, P., and Zanier, F., "Ariane 5 MPS Chamber Pressure Oscillations Full Scale Firings Results Analysis and Further Studies," 30th AIAA Joint propulsion Conference, Indianapolis, IN, AIAA Paper 94-3068, June 1994.

[3] Flatau, A., and Van Moorhem, W. K., "Vortex Shedding Induced Sound Inside a Cold-Flow Simulation of Segmented Chamber," *Journal of Propulsion and Power*, Vol. 19, No. 2, 2003, pp. 287–296. doi:10.2514/2.6110

[4] Griffond, J., and Casalis, G., "On the Dependence on the Formulation of Some Nonparallel Stability Applied to the Taylor Flow," *Physics of Fluids*, Vol. 12, No. 2, 2000, pp. 466–468. doi:10.1063/1.870323

[5] Zhao, Q., and Kassoy, D. R., "The Generation and Evolution of Unsteady Vorticity in a Model of a Solid Rocket Motor Engine Chamber," 32nd Aerospace Sciences Meeting and Exhibit, AIAA Paper 1994-779, Jan. 1994.

[6] Brown, R. S., Dunlap, R. S., Young, W., and Waugh, R. C., "Vortex Shedding as a Source of Acoustic Energy in Segmented Solid Rocket Motor," *Journal of Spacecraft and Rockets*, Vol. 18, No. 4, 1981, pp. 312–319. doi:10.2514/3.57822

[7] Lupoglazoff, N., and Vuillot, F., "Numerical Simulations of Parietal Vortex-Shedding Phenomenon in a Cold Flow Set-Up," 34th AIAA/ASME/SAE/ASEE Joint Propulsion Conference and Exhibit, AIAA Paper 1998-3220, Cleveland, OH, July 1998.

[8] Nguyen, C. C., Plourde, F., and Doan-Kim, S., "Analysis of Injecting Wall Inclination on Coupling Mechanisms in Segmented Chamber," *Journal of Propulsion and Power*, Vol. 24, No. 2, 2008, pp. 213–223. doi:10.2514/1.29551

[9] Najjar, F. M., Balachandar, S., Alavilli, P. V. S., and Ferry, J., "Computations of Two-Phase Flow in Aluminized Solid Propellant Rockets," 36th AIAA/ASME/SAE/ASEE Joint Propulsion Conference, AIAA Paper 2000-3568, Huntsville, AL, July 2000.

[10] Fiedler, R., Namazifard, A., Campbell, M., and Xu, F., "Detailed Simulations of Propellant Slumping in the Titan IV SRMU PQM-1," 42nd AIAA/ASME/SAE/ASEE Joint propulsion Conference and Exhibit, Sacramento, CA, AIAA Paper 06-4592, July 2006.

[11] Fouilhac, L., Gutmark, E. J., and Garrison, T. J., "Interaction of Flow/Structure in a Jet Flowing Through a Flexible Membrane," AIAA Fluid Dynamics Conference, AIAA Paper 97-1911, 1997.

[12] Plourde, F., Couton, D., and Doan-Kim, S., "Analysis of Energy Transfers of a Sheared Flow Generated by Wall Injection," *Experiments in Fluids*, Vol. 26, 1999, pp. 222–232. doi:10.1007/s003480050283

[13] Vetel, J., Plourde, F., and Doan Kim, S., "Dynamics of an Internal Flowfield Driven by Two Hydrodynamic Instabilities," *AIAA Journal*, Vol. 41, No. 3, 2003, pp 424–435. doi:10.2514/2.1993

[14] Vetel, J., Plourde, F., and Doan Kim, S., "Amplification of a Shear-Layer Instability by Vorticity Generation at an Injecting Wall," *AIAA Journal*, Vol. 42, No. 1, 2004, pp. 35–46. doi:10.2514/1.9028

[15] Staab, P. L., and Kassoy, D. R., "Three-Dimensional Flow in a Cylinder with Sidewall Mass Addition," *Physics of Fluids*, Vol. 14, No. 9, 2002, pp. 3141–3159. doi:10.1063/1.1492283

[16] Fouilhac, L., Gutmark, E. J., and Garrison, T. J., "Interaction of Flow/Structure in a jet Flowing Through a Flexible Membrane," 28th AIAA/Fluid Dynamics Conference, AIAA Paper 91-1911, 1997.

[17] Vetel, J., Plourde, F., Doan-Kim, S., and Prevost, M., "Cold Gas Simulation of the Influence of Inhibitor Shape in Combustor Combustion," *Journal of Propulsion and Power*, Vol. 21, No. 6, 2005, pp. 1098–1106. doi:10.2514/1.7445

S. Son
Associate Editor